ORIGINAL PAPER

Electrochemical properties and extraction of Dy on liquid Sn electrode in LiCl–KCl molten salt

Wenlong Li[1] · Xin Zhang[1] · Ji Wang[1] · Lifeng Chen[1] · Quanzhang Sun[1] · Wei Han[2] · Mei Li[2] · Yuezhou Wei[1]

Abstract

To extract dysprosium (Dy) from LiCl–KCl molten salt, the electrochemical properties of Dy on liquid Sn electrode were explored by various electrochemical methods such as cyclic voltammetry (CV), chronopotentiometry (CP), and coulometric titration (CT). The Dy-Sn solid solution ((Dy-Sn)$_{solution}$) was formed when the Dy was deposited on liquid Sn. The electrode process is a reversible reaction controlled by diffusion, and the diffusion coefficient of Dy(III) in LiCl–KCl molten salt was measured in the order of 10^{-5} cm^2 s^{-1}. CT and CP were used to assess the solubility and diffusion coefficient of Dy in liquid Sn, respectively. Meanwhile, the co-deposition of Dy(III) and Sn(II) was analyzed by CV and square wave voltammetry (SWV) to obtain the Dy-Sn intermetallic compounds, and four electrochemical signals related to Dy-Sn intermetallic compounds were observed. In addition, the feasibility of extracting Dy using liquid Sn electrode was verified by galvanostatic electrolysis (GE) and potentiostatic electrolysis (PE), and the products were characterized by XRD and SEM–EDS. The Dy-Sn alloys prepared by PE and GE consisted of DySn$_2$ and (DySn$_3$ + DySn$_2$), respectively.

Keywords LiCl–KCl molten salt · Electrochemical properties · Liquid Sn electrode · Electrochemical extraction · Dy-Sn alloys

Introduction

Nuclear power, as a kind of high-energy density, clean, and low-carbon power, has become an important way to resolve the increasing energy crisis [1–4]. However, only a small fraction of uranium is utilized during nuclear reaction and large amounts of spent nuclear fuel (SNF) are produced from the reactor, including about 94% uranium, transuranic, and fission products (FP) [5–7]. Thus, the recovery of uranium from SNF in an effective and safe manner has been a key issue for the sustainable development of nuclear energy. Pyrochemical reprocessing is a

promising technology to recover uranium from SNF and the key step is electrolytic refining, where the molten salts such as LiCl–KCl usually are used as electrolyte owing to its high thermal resistance, high radiation resistance, and high solubility to uranium and FP [8–12]. In the electrolytic refining, uranium and transuranic are electrodeposited on solid stainless steel and liquid cadmium electrodes, respectively. However, lanthanides (Lns) are remained in the molten salt, which account for about 1/4 of FP and possess the similar chemical properties with actinides [13–16]. With the deposition of uranium and transuranic, Lns are gradually accumulated in molten salts, which will change the molten salt composition and contaminate the recovered uranium. In addition, Lns, known as a neutron poison, have a large neutron absorption cross-section which can reduce the neutron efficiency of nuclear reactor core [17–19]. Thus, Lns must be extracted from molten salts in order to purify the molten salts and increase neutron utilization during nuclear reaction process.

The extraction of Lns from molten salts is affected by many factors, such as electrode material, temperature, and ion concentration [8, 20, 21]. The deposition potential of Lns on electrode is the key to electrochemical extraction, and the Lns can form different alloys on various

✉ Wei Han
weihan@hrbeu.edu.cn

✉ Mei Li
meili@hrbeu.edu.cn

1 School of Nuclear Science and Technology, University of South China, 28 Changsheng West Road, Hengyang 421001, People's Republic of China

2 Key Laboratory of Superlight Materials and Surface Technology, Ministry of Education, College of Materials Science and Chemical Engineering, Harbin Engineering University, Harbin 150001, People's Republic of China

electrodes, which results in the different deposition potentials. Thus, electrode materials are particularly important in the electrolysis process. In recent decades, in order to improve the extraction efficiency of Lns, the electrochemical behavior and extraction of Lns in molten salts have been studied on disparate active electrodes, including Cu [22–25], Al [26–31], Mg [32–35], Ni [36–38], Zn [39–41], Ga [42–44], Bi [45–47], Sn [48, 49], Pb [50–53], and Cd [54–56]. Although the electrochemical behavior and extraction of Lns have been studied extensively on solid Cu, Al, Mg, and Ni electrodes, the diffusion rate of deposited Lns in solid electrode is very slow, which is not conducive to extraction. Thus, the low melting point metals Zn, Ga, Bi, Sn, Pb, and Cd have attracted much attention from researchers, because the low melting point metals are liquid under experimental conditions, which is more conducive to the diffusion of Lns from the electrode surface to interior. Jiao et al. analyzed the advantages of liquid electrode such as strong alloying effect, strong depolarization effect, and excellent selective separation [57]. Han et al. compared the kinetic, thermodynamic, and extraction data of Y on solid copper and liquid zinc electrodes, and found that Y was more easily deposited on liquid Zn electrode under the same condition [58]. Metallic tin (Sn) has the advantages of low melting point, low vapor pressure, low toxicity, and suitable price, which makes it a good candidate for the extraction of Lns from molten salts. The co-deposition of Sn(II) and Lns ions (Pr(III) and Sm(III)) on W electrode was studied, and the extraction of Pr and Sm on liquid Sn electrode was conducted [48, 49]. However, the electrochemical properties of Lns on liquid Sn electrode were less studied, and the Lns with large atomic numbers have not been studied. In addition, the operation conditions significantly influence the feasibility of extraction. It is of crucial importance to obtain the electrochemical behavior of Lns on Sn electrode for the understanding of the process and the design of the separation cell. Thus, the electrochemical properties and extraction of Lns on liquid Sn electrode need to be supplemented.

In this paper, dysprosium (Dy) with a large atomic number was selected as the representative of Lns to investigate the electrochemical properties and extraction in detail on liquid Sn electrode. Meanwhile, the co-deposition of Dy(III) and Sn(II) on inert W electrode was firstly explored. Electrochemical techniques such as CV, CP, CT, and SWV were used to investigate the reversibility of electrode reaction, the diffusion coefficient, the solubility of Dy on liquid Sn electrode, and the formation mechanism of Dy-Sn intermetallic compounds. Based on the results mentioned above, the electrochemical extraction of Dy on liquid Sn electrode was conducted by PE and GE. The composition, elemental distribution, and microtopography of samples were analyzed by

X-ray diffraction (XRD) and scanning electron microscopy (SEM) with energy-dispersive spectrometry (EDS).

Experimental

Reagents and molten salt preparation

Due to the melting point of eutectic salt lower than that of single salt, 40.8 mol% KCl (analytical reagent grade) and 59.2 mol% LiCl (analytical reagent grade) were mixed in an alumina crucible to form the eutectic salt, which was chosen as the electrolyte. Then, the LiCl–KCl molten salt was dried in a muffle furnace for 48 h at 473 K to remove water. Before the experiment, the molten salt was melted at 773 K in an electric furnace, and then, pre-electrolysis was conducted at −2.2 V for 4 h in order to remove other impurities. According to the experimental requirements, LiCl–KCl-DyCl$_3$ and LiCl–KCl-DyCl$_3$-SnCl$_2$ molten salts were prepared by adding different masses of DyCl$_3$ and SnCl$_2$ to LiCl–KCl molten salt.

Apparatus and electrodes

In this work, all electrochemical tests were conducted by Autolab PGSTAT 302 N with Nova 1.10 software in a glove box. The three-electrode system was used to analyze electrode reactions and extract Dy on Sn electrode. The working electrodes were W wire (99.99%, $\varphi = 1$ mm) and liquid Sn. Herein, the W wire was polished with 5000 mesh sandpaper and then washed with ethanol and hydrochloric acid. Liquid Sn electrode was prepared by adding some Sn particles to an alumina crucible, and the tungsten wire inserted into liquid Sn serves as an electric lead. The reference electrode was Ag/Ag$^+$, which was prepared by inserting a Ag wire into LiCl–KCl-AgCl (1 wt%) molten salt contained in an alumina tube, and a spectral pure graphite rod served as counter electrode.

Electrochemical measurement and product characterization

The electrode reactions of Dy on liquid Sn electrode and co-deposition of Dy(III) and Sn(II) on W electrode were studied by CV, SWV, CP, and CT. GE and PE were performed to prove the feasibility of extracting Dy on liquid Sn electrode. After the electrolysis, the product was removed from the molten salt and washed with deionized water, and then analyzed by XRD and SEM–EDS in order to obtain the phase constitution, elemental distribution, and content. In addition, the concentration of Dy(III) in LiCl–KCl melt was detected using an inductively coupled plasma atomic emission spectrometer (ICP-AES).
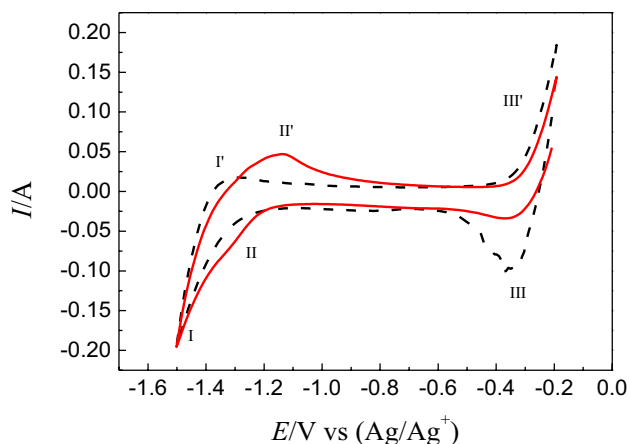
Fig. 1 CV curves obtained in LiCl–KCl melts before (black dashed line) and after (red solid line) adding DyCl$_3$ at 773 K. Working electrode: liquid Sn; scanning rate: 0.1 V s^{-1}; electrode area: 1.256 cm.^{2}

Results and discussion

Electrochemical properties of Dy(III) on liquid Sn electrode

Firstly, the electrode reaction of Dy on liquid Sn electrode was studied applying CV which is a typical electrochemical method. Figure 1 shows the CV curves measured in LiCl–KCl (black dashed line) and DyCl$_3$-LiCl–KCl (red solid line) molten salt on liquid Sn electrode. Two pairs of redox signals, I/I′ and III/III′, were detected in black dashed line, which are attributed to the deposition and dissolution of Li and Sn, respectively [49]. When DyCl$_3$ was added to the LiCl–KCl molten salt, a pair of new redox peaks II/II′ is observed at −1.29 V/−1.14 V besides I/I′ and III/III′. Compared to the LiCl–KCl molten salt, only Dy(III) was introduced into the molten salt. Thus, the redox peaks II/II′ should be correlated with the formation and oxidation of Dy on liquid Sn electrode, and the deposition potential is more positive than that of Dy on W electrode [21], indicating that the Dy(III) can occur under-potential deposition on liquid Sn electrode. The reduction potential of Dy(III) on Cu, Mg, and Pb electrodes is about −1.45 V, −1.80 V, and −1.35 V [25, 50, 59], respectively, which are more negative than the reduction potential of Dy(III) on the liquid Sn electrode, proving Dy is easier to deposit on liquid Sn electrode. Besides, a small amount of Dy was deposited on the liquid Sn electrode during CV scanning, and the maximum solubility of Dy in liquid Sn cannot be reached. Hence, the redox peaks II/II′ are preliminarily inferred to be the formation and subsequent oxidation of (Dy-Sn)$_{solution}$, which is similar to the reduction of Pr on liquid Sn electrode [49], and the corresponding redox reaction is expressed as:

$$Dy(III) + 3e^- + Sn = (Dy - Sn)_{solution} \quad (1)$$
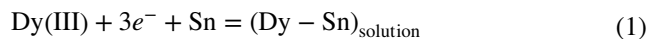
In order to verify the formation of (Dy-Sn)$_{solution}$, reverse chronopotentiometry (RCP) was carried out at ± 30 mA and the corresponding curves are shown in Fig. 2. During the deposition and oxidation, the platforms II and II′ can be observed, which are related to the deposition and dissolution of Dy on liquid Sn electrode, respectively. Furthermore, an additional platform III′ appears except for II′ during the oxidation process, which is correlated with the dissolution of metallic Sn. As we all know, when the electrode reaction is soluble-insoluble system, the reduction product is attached to the surface of electrode, and the reduction product can be oxidized completely, indicating the reduction time is equal to oxidation time. However, for soluble-soluble system, most of the reduction product will diffuse into the liquid electrode or solution, and the reduction product cannot be oxidized completely. According to the RCP curves, the deposition and dissolution time of Dy on liquid Sn electrode can be obtained to be 9.68 and 2.83, respectively. It can be found that the deposition time is almost three times longer than the dissolution time, proving that the (Dy-Sn)$_{solution}$ was formed on the liquid Sn electrode [60].

To study the reversibility and control procedure of Dy on liquid Sn electrode, CV with different scanning speeds was performed in DyCl$_3$-LiCl–KCl molten salt, and the result is presented in Fig. 3a. The relationship of cathode peak potential to scanning speed is shown in Fig. 3b (blue dot), and it can be clearly observed that the peak potential of peak II almost unchanged with the change of scanning speed, indicating that the reduction process of Dy(III) on the liquid Sn electrode is reversible. In addition, the change of peak current with square root of scan rate is displayed in Fig. 3b (black dot), which is a line through the origin, demonstrating the reduction of Dy(III) on liquid Sn electrode is
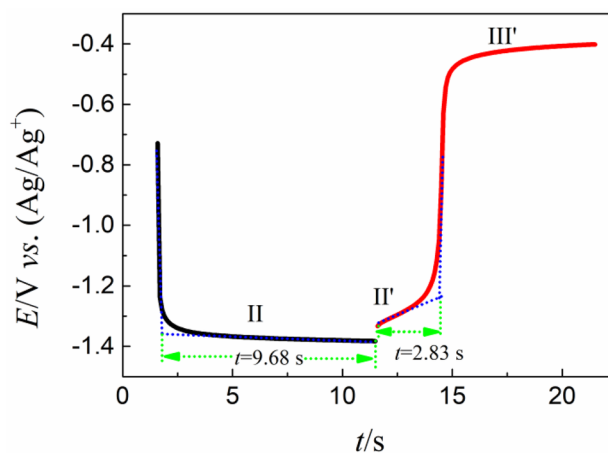

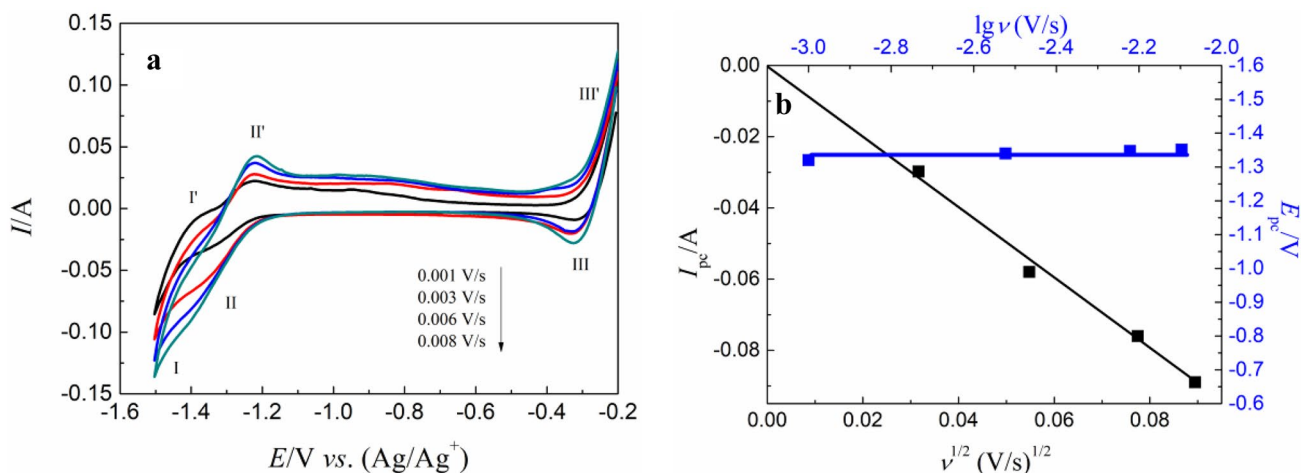**Fig. 2** RCP curves obtained at ± 30 mA on liquid Sn electrode

Fig. 3 **a** CV curves with different scanning rates recorded in LiCl–KCl-DyCl$_3$. **b** The relationship maps of E_{pc} vs lg$v$ and I_{pc} vs $v^{1/2}$. Working electrode: liquid Sn; electrode area: 1.256 cm^2; temperature: 773 K

controlled by diffusion. Thus, the electrode process of Dy on liquid Sn electrode is a quasi-reversible reaction controlled by diffusion.

For the soluble-soluble reversible process controlled by diffusion, the diffusion coefficient can be computed by the Randles–Sevcik equation [18]:

$$I_p = 0.4463(nF)^{3/2}(RT)^{-1/2}AC_0v^{1/2}D^{1/2} \qquad (2)$$

where I_p designates the cathode peak current derived from CV curve (A), n is the electron transfer number, F denotes the Faraday constant (96,500 C mol^{-1}), R is the universal gas constant (8.314 J mol^{-1} K^{-1}), T designates temperature (773 K), A is the working electrode area (1.256 cm^2), C_0 is the concentration of Dy(III) in molten salt (2.86×10^{-4} mol cm^{-3}), v is the scanning speed (V s^{-1}), and D is the diffusion coefficient (cm^2 s^{-1}). According to the Randles–Sevcik equation, the peak current should be proportional to the square root of scan rate, which corresponds to Fig. 3b. Based on the slope of the black line in Fig. 3b and Eq. 2, the diffusion coefficient of D(III) in molten salt was calculated to be 1.01×10^{-5} cm^2 s^{-1}, which is consistent with 1.48×10^{-5} cm^2 s^{-1} obtained by Castrillejo et al. [61]. The difference may be due to the different concentrations of Dy(III) and different working electrodes. In addition, the diffusion coefficient of D(III) at 773 K was calculated by the relationship of temperature and diffusion coefficient, which may also cause the difference of diffusion coefficient.

Solubility and diffusion coefficient of Dy atom in liquid Sn

The Dy-Sn intermetallic compounds will be formed after the maximum solubility of Dy in liquid Sn is reached, which

will hinder the diffusion of Dy atom into liquid Sn. Thus, the solubility of Dy atom in liquid Sn plays an important role for the extraction of Dy from LiCl–KCl molten salt. In order to obtain the solubility of Dy atom in liquid Sn, the CT was conducted. Figure 4 displays the CT curves, which is made up of CP and open circuit (OC) curves. The same color is a group, and the CP and OC curves are on the left and right, respectively. The CP was used to deposit Dy on liquid Sn, and OC curve was applied to measure the equilibrium potential of liquid Sn cathode. To avoid the reduction of Li(I) on liquid Sn electrode, the deposition current gradually decreased from -0.2 to -0.08 A. Simultaneously, the OC curve was recorded immediately after each deposition. In Fig. 4, it can be found that the OC curve (from red to yellow) gradually shifts to the negative direction with the deposition of Dy on liquid Sn, which is caused by incremental activity of Dy as
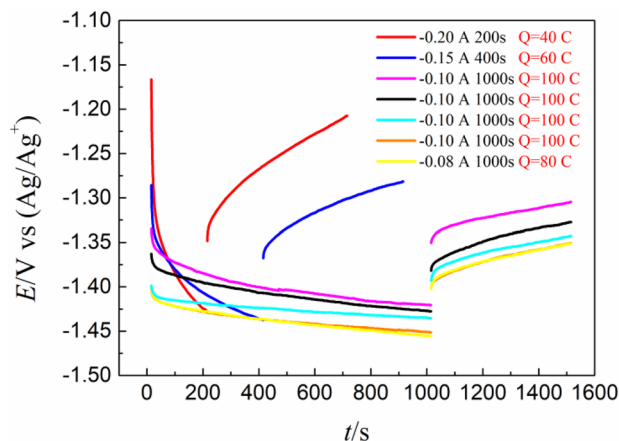

Fig. 4 CT curves with different currents at 773 K in LiCl–KCl-DyCl$_3$ melts
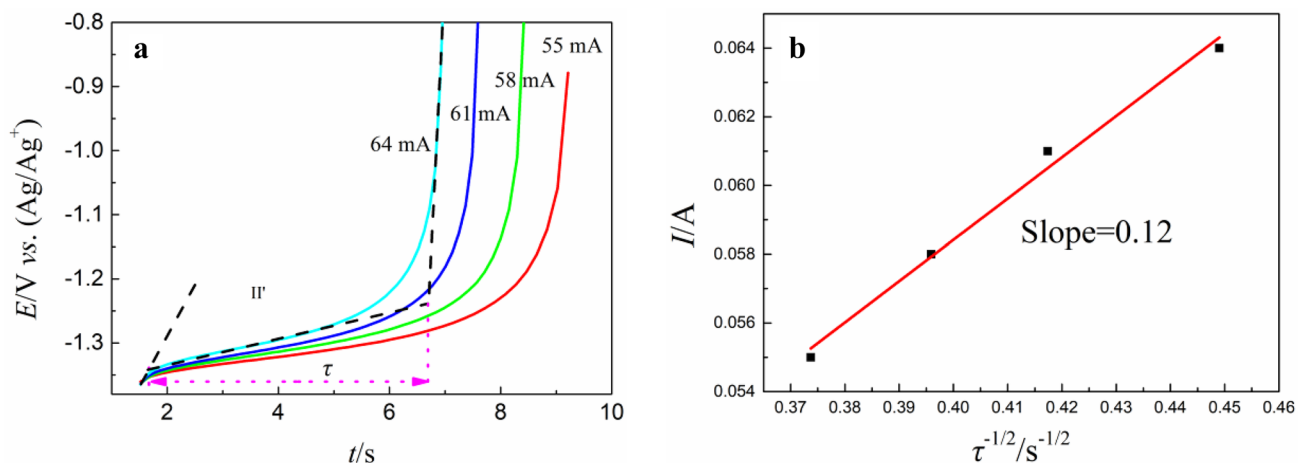
Fig. 5 **a** CP curves of Dy in liquid Sn at 773 K, current: 55–64 mA, electrode area: 1.256 cm². **b** Relationship of current and reciprocal square root of transition time

the content of Dy in liquid Sn increases. However, when the total charge reaches 500 C and 580 C calculated through multiplying the current by time, the OC curves almost coincide, indicating the Dy-Sn intermetallic compound was formed when the charge reaches 500 C. Consequently, the maximum solubility of Dy in liquid can be reckoned according to the electricity (500 C) and mass (5 g) of Sn, and the value is 3.95×10^{-2} (mole fraction), which is higher than the solubility of Pr (7.48×10^{-3}) and Ce (1.74×10^{-2}) in liquid Bi [62].

The diffusion coefficient of Dy atom in liquid Sn has a strong influence on the mass transfer of the electrode process. Thus, the CP was performed at various currents to measure the diffusion coefficient, and the curves were recorded in Fig. 5a. Firstly, GE was conducted at -0.08 A for 400 s and the content of Dy in liquid Sn was calculated to be 2.60×10^{-3}, which is less than 3.95×10^{-2}, demonstrating

the (Dy-Sn)$_{solution}$ was formed. Then, CP was performed at different currents after potential stabilization. As shown in Fig. 5a, the platform II′ is corresponding to the dissolution of Dy according to the CV and RCP curves, and the transition time was obtained based on the CP curves. It can be found that the transition time gradually decreased when the current increase. Figure 5b presents the relationship of current and reciprocal square root of transition time, which is linear. The result is consistent with the Sand equation expressed by Eq. 3 [63–65].

$$I = \frac{nFAC(D\pi)^{1/2}}{2}\tau^{-1/2} \tag{3}$$

where I is the applied current (A), C denotes the concentration of Dy atom in liquid Sn (mol cm^{-3}), τ presents the transition time (s), and n, F, A, and D have the same meaning as
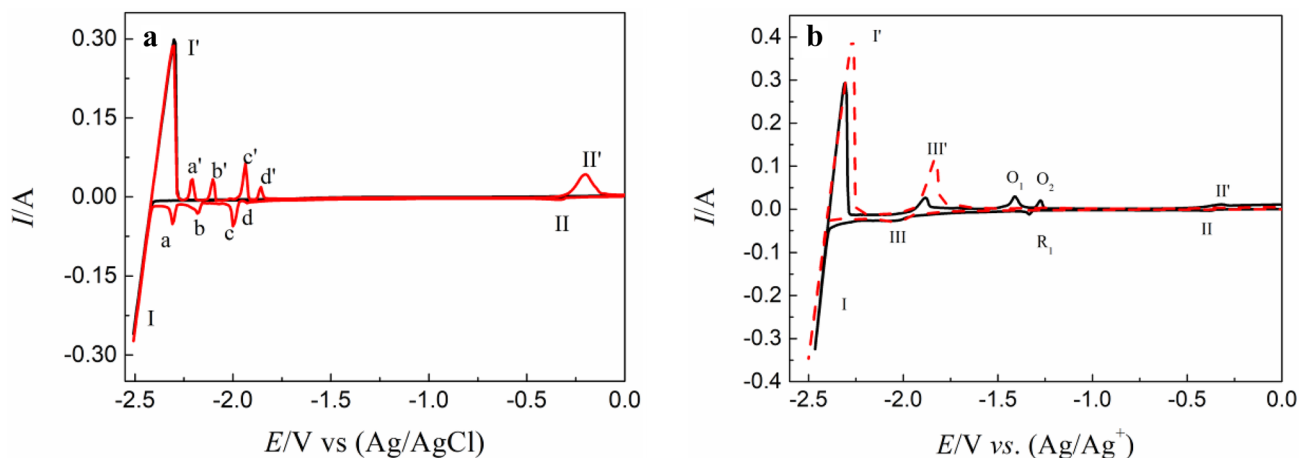

Fig. 6 CV curves recorded in **a** LiCl–KCl and LiCl–KCl-DyCl$_3$ melts and **b** LiCl–KCl-DyCl$_3$ melts before (red dashed line) and after adding SnCl$_2$ (black solid line). Scanning rate: 0.1 V s^{-1}; working electrode: W; temperature: 773 K

in Eq. 2. According to the slope of line in Fig. 5b and Eq. 3, the diffusion coefficient of Dy atoms in the liquid Sn can be calculated to be 5.35×10^{-6} cm^2 s^{-1}, which is smaller than the value acquired in molten salt, indicating the diffusion of Dy atoms in liquid Sn is slower than that of Dy(III) in molten salt.

Co-deposition of Dy(III) and Sn(II) on W electrode

To explore the formation mechanism of Dy-Sn intermetallic compounds, the co-deposition of Dy(III) and Sn(II) was conducted on W electrode. Firstly, the SnCl$_2$ was added into LiCl–KCl to study the Li-Sn alloy, shown in Fig. 6a. Only a pair of redox signals I/I′ is found when the SnCl$_2$ is absent (black line in Fig. 6a), which is attributed to the reduction and oxidation of Li on W electrode. When the SnCl$_2$ was added into the molten salt (red line in Fig. 6a), five pairs of redox peaks are observed except for I/I′, where II/II′ (−0.38 V/−0.32 V) correspond to the deposition and dissolution of Sn. The peaks a/a′ (−2.31/−2.21 V), b/b′ (−2.18/−2.10 V), c/c′ (−2.00/−1.94 V), and d/d′ (−1.93/−1.86 V) located between I/I′ and II/II′ are ascribed to the formation and oxidation of Li-Sn alloys. The peak potentials of Sn-Li intermetallic compounds are more negative than the value of Bi-Li intermetallic compounds [47], illustrating that Li is more likely to be deposited on Bi electrode. The deposition of Li will reduce the current efficiency of extraction.

However, it can be found from the black solid line in Fig. 6b that the peaks of Li-Sn alloys disappeared when the DyCl$_3$ was added into LiCl–KCl-SnCl$_2$. The reason may be that all the deposited Sn react with Dy to form Dy-Sn alloys, and there is not enough Sn to react with Li. The same phenomenon was also recorded in LiCl–KCl-SnCl$_2$-PrCl$_3$ molten salt when OCP measurement was conducted [49]. In Fig. 6b, the red dashed line reveals the CV curve recorded in LiCl–KCl-DyCl$_3$ molten salt, and the peaks III/III′ are related to the deposition and dissolution of Dy [42]. In the black solid line, a new reduction peak (R$_1$) and two oxidation peaks (O$_1$ and O$_2$) were detected besides I/I′, II/II′, and III/III′ after adding SnCl$_2$ to LiCl–KCl-DyCl$_3$ molten salt, which are associated with the formation and subsequent dissolution of Sn-Dy intermetallic compounds, respectively. The formation process can be described by the following equation:

$$x\text{Sn(II)} + \text{Dy(III)} + (2x + 3)\text{e}^- = \text{DySn}_x \tag{4}$$
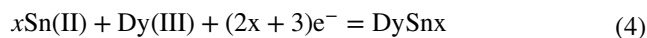
To confirm the corresponding relationship between the reduction and oxidation peaks, CV with different termination potentials was performed. It can be seen from Fig. 7 that the six reduction peaks II (−0.34 V), III (−2.02 V), R$_1$ (−1.32 V), R$_2$ (−1.36 V), R$_3$ (−1.67 V), and R$_4$ (−1.92 V) and the five oxidation peaks II′ (−0.24 V), III′ (−1.87 V), O$_1$ (−1.24 V), O$_2$ (−1.38), and O$_3$ (−1.69 V) are observed when
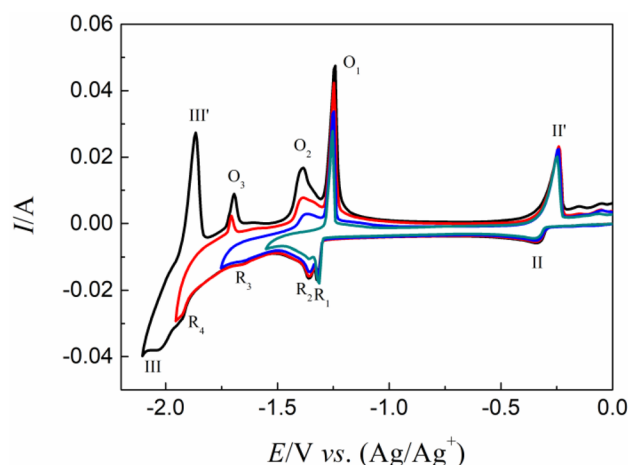

Fig. 7 CV curves with different termination potentials in LiCl–KCl-DyCl$_3$-SnCl$_2$ melts. Scanning rate: 0.1 V s^{-1}; working electrode: W; temperature: 773 K

the termination potential is −2.11 V. Besides II/II′ and III/III′ mentioned above, the other peaks are related to the formation and dissolution of Dy-Sn intermetallic compounds. When the termination potential was changed from −2.11 to −1.55 V, the reduction peaks III, R$_4$, and R$_3$ and oxidation peaks III′, O$_3$, and O$_2$ disappear successively, indicating that the peaks III, R$_4$, and R$_3$ correspond to the peaks III′, O$_3$, and O$_2$, respectively. Nevertheless, when the termination potential is −1.55 V, the two reduction peaks R$_1$ and R$_2$ and one oxidation peak O$_1$ are observed, which may be caused by the fact that the oxidation peaks of R$_1$ and R$_2$ are too close to separate.

SWV, a more sensitive electrochemical technique than CV, was used to explore further formation of Dy-Sn intermetallic compounds. Figure 8 shows the cathodic and anodic
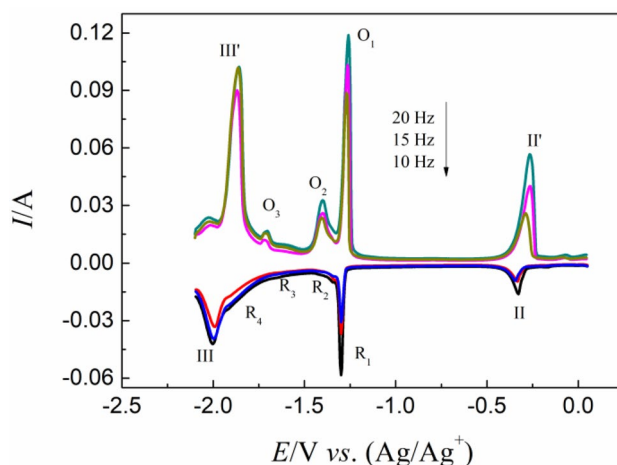

Fig. 8 Cathodic and anodic SWV curves with different frequencies in LiCl–KCl-DyCl$_3$-SnCl$_2$ melts. Step potential: 5 mV; amplitude: 25 mV
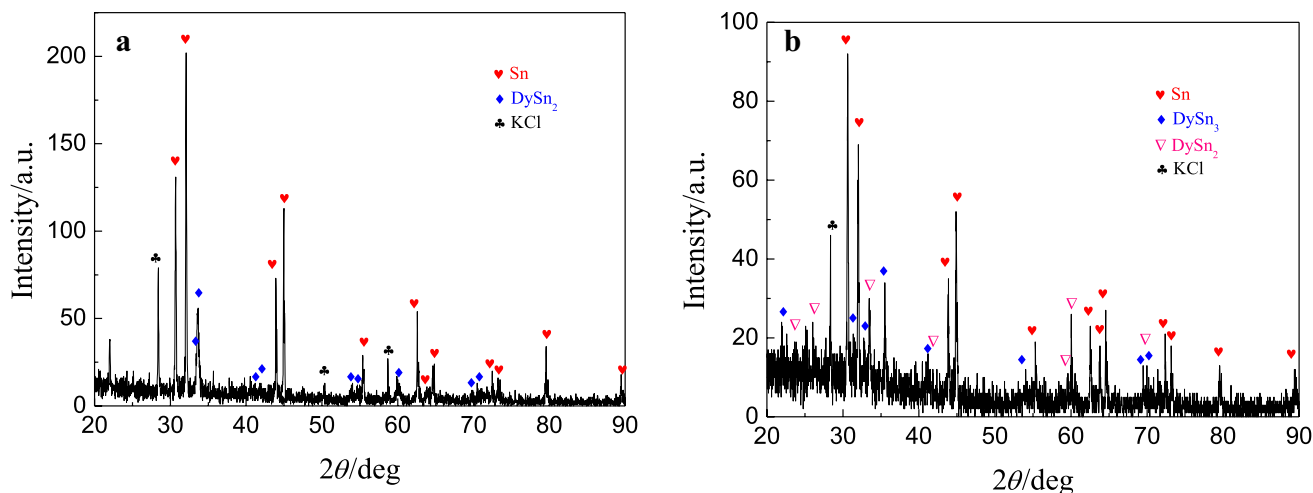
Fig. 9 XRD maps of products obtained by **a** PE (−1.30 V) and **b** GE (−0.08 A) for 7 h on liquid Sn electrode in LiCl–KCl-DyCl$_3$ melts

SWV curves with different frequencies. Four reduction peaks between II and III are observed in cathodic SWV curves and three oxidation peaks between II′ and III′ are observed in anodic SWV curves, which is consistent with the result of CV, demonstrating that four Sn-Dy intermetallic compounds can be formed under the experimental conditions. Moreover,

the peak currents of Sn-Dy intermetallic compounds gradually increase with the increase of frequency, indicating that the electrode reaction rate increases. Meanwhile, it can be clearly seen that the peak potentials of Sn-Dy intermetallic compounds hardly change in the wake of the frequency, proving that the redox process is reversible.

Fig. 10 a–f SEM–EDS maps of product obtained at −1.30 V for 7 h in LiCl–KCl-DyCl$_3$ melts
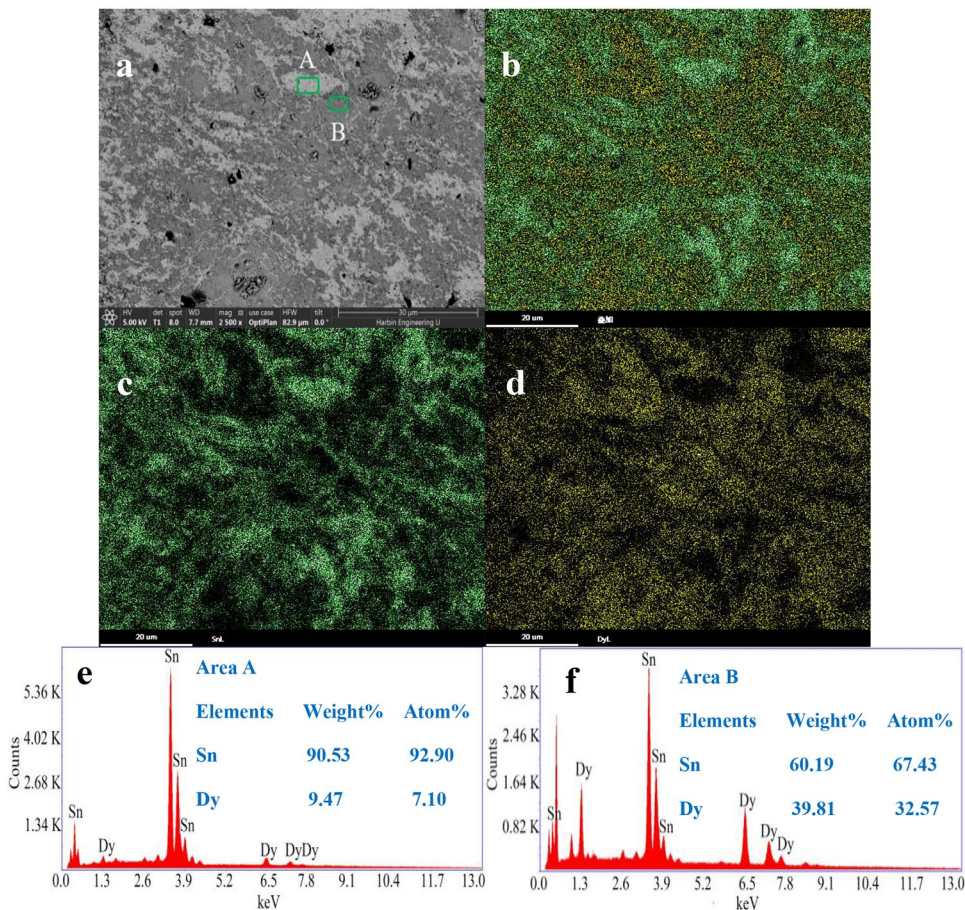
## Electrochemical extraction of Dy on liquid Sn electrode

According to the results discussed above, the Dy can be extracted from LiCl–KCl-DyCl₃ molten salt using liquid Sn electrode and form Dy-Sn alloys. Thus, the PE (−1.30 V) and GE (−0.08 A) were used for the extraction of Dy to verify the experimental result. The compositions of the samples were analyzed by XRD, shown in Fig. 9. It can be seen from Fig. 9a that the $DySn_2$ was obtained after PE for 7 h. From Fig. 9b, it can be found that the phase constitution of Dy-Sn alloy is $DySn_3$ and $DySn_2$ after GE for 7 h. Furthermore, the KCl was detected in the samples of PE and GE, which is mainly caused by incomplete cleaning of samples.

In addition, the products were also analyzed by SEM with EDS. Figures 10 and 11 show the SEM–EDS maps obtained at −1.30 V for 7 h and −0.08 A for 7 h, respectively. As shown in Fig. 10a, white and gray areas were observed, indicating the composition of two areas is different. It can be clearly found from Fig. 10b–d that the white area in Fig. 10a is mainly composed of Sn metal, while the Dy element is mainly distributed in the gray area. In order to quantify the element content of different regions, EDS was performed to analyze the representative areas (A) and (B) in Fig. 10a. In

Fig. 10e, f, the atomic ratios of Sn and Dy are 92.9:7.1 in the (A) area and 67.43:32.57 in the (B) area. The atomic ratio of Sn and Dy in the (B) area is close to 2:1, which is consistent with that of XRD. Thus, the sample prepared at −1.30 V is made up of Sn and $DySn_2$.

Figure 11 shows the SEM–EDS of the product prepared by GE in LiCl–KCl-DyCl₃ molten salt. The SEM image shown in Fig. 11a also displays two areas, white and gray, and the white area is larger than the gray area. The results of EDS shown in Fig. 11b–d certify that the product consists of Sn and Dy elements. Combined with Fig. 11a, it can be found that the Dy is mainly distributed in the gray area and Sn in the white area. Figure 11e, f display the EDS analysis of (A) and (B) shown in Fig. 11a, and the atomic ratios of Sn:Dy are 98.85:1.15 and 83.85:16.15, respectively, indicating the Dy extracted by GE is less than that of PE in the same time. The reason was attributed to the gradual decrease of Dy(III) in molten salt during GE, which caused the potential to move in the negative direction. When the potential was able to reduce Li(I), part of Li was also deposited on liquid Sn, which resulted in the decrease of current efficiency. However, the potential remained unchanged during PE, and only Dy(III) was reduced in the whole electrolysis process. Thus, the efficiency of PE is higher. Judging from the results of XRD and SEM–EDS, the

Fig. 11 a–f SEM–EDS maps of product obtained at −0.08 A for 7 h in LiCl–KCl-DyCl₃ melts
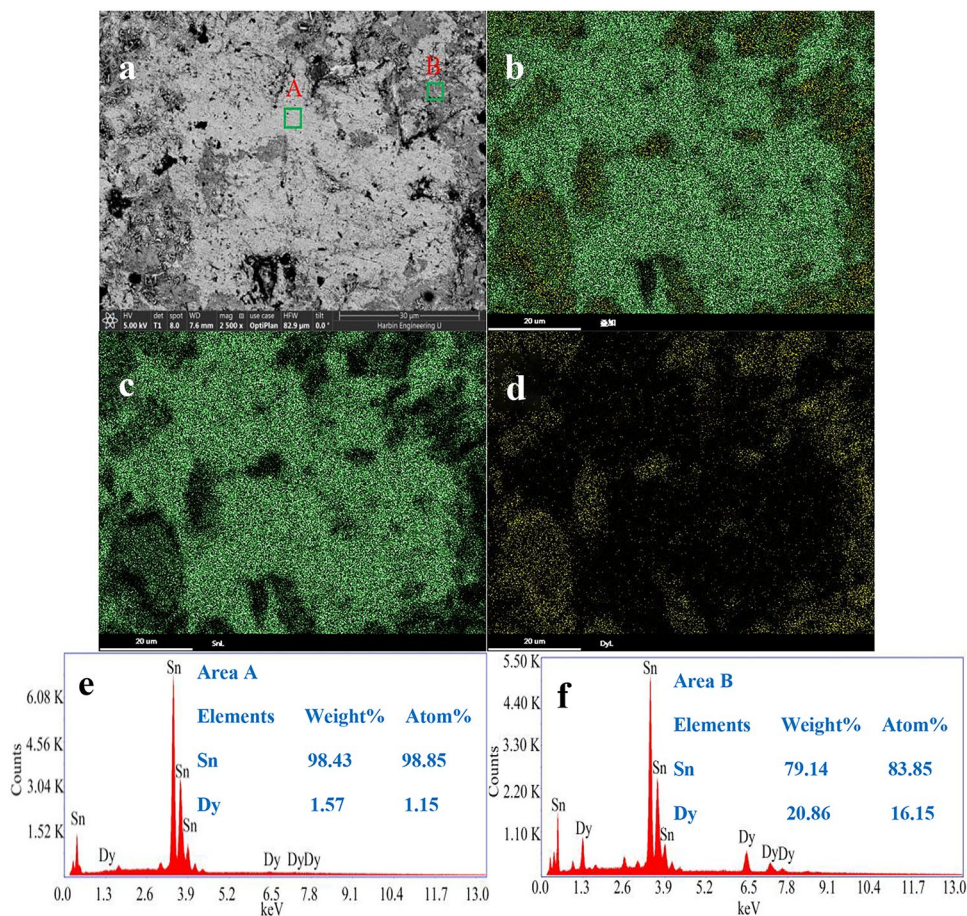
sample obtained by GE is made up of Sn, DySn$_3$, and DySn$_2$. In addition, it can be seen clearly from Figs. 10b and 11b that the reduced metal Dy is distributed throughout the metallic Sn, indicating Dy can fully diffuse in liquid Sn electrode. When the extraction of Dy was conducted on solid Cu [25], Al [28], Mg [59], and Ni [66] electrodes, an obvious alloy layer was formed outside the metal matrix, demonstrating the diffusion of Dy in solid electrodes is greatly hindered. The experimental results demonstrate that metallic Sn is a good electrode material for extracting Dy, which can be realized by PE and GE, and the efficiency of PE is higher.

Conclusion

The electrochemical behaviors of Dy on liquid Sn electrode and co-deposition of Dy(III) and Sn(II) were explored in LiCl–KCl molten salt. The results of CV and RCP showed that the (Dy-Sn)$_{solution}$ was formed when Dy was deposited on liquid Sn: $Dy(III) + 3e^- + Sn = (Dy-Sn)_{solution}$. The electrode process of Dy on liquid Sn electrode was found to be a reversible reaction controlled by diffusion, and the diffusion coefficient of Dy(III) in LiCl–KCl molten salt was calculated to be 1.01×10^{-5} cm^2 s^{-1}. The diffusion coefficient of Dy atom in liquid Sn was also measured to be 5.35×10^{-6} cm^2 s^{-1} by CP, which is smaller than the value of Dy(III) in molten salt. The solubility of Dy in liquid Sn was evaluated to be 3.95×10^{-2} (mole fraction) using CT at 773 K. In addition, the co-deposition mechanism of Dy(III) and Sn(II) was analyzed. The result showed that four Dy-Sn intermetallic compounds can be formed by co-deposition. Meanwhile, the extraction of Dy was conducted by PE (-1.3 V) and GE (-0.08 A) using liquid Sn as working electrode, and the phase constitution of Dy-Sn alloy was analyzed to be DySn$_2$ and (DySn$_3$ + DySn$_2$), respectively, indicating the efficiency of PE is higher than that of GE. Thus, it is feasible to extract Dy using liquid Sn electrode, which could supplement the experimental data of non-aqueous reprocessing and accelerate the application of molten salt electrolysis in engineering.

Data availability The data that support the findings of this study are available from the corresponding author upon reasonable request.

References

1. Xu XJ, Wang XP, Smolenski V, Mi WS, Yan YD, Novoselova A, Xue Y, Ma FQ, Zhang ML, Zhang XM, Zhu K (2022) Electrochemical extraction of uranium from U$_3$O$_8$ by preparing flower-shaped Al-U intermetallics in LiCl-KCl-AlCl$_3$ melts. J Nucl Mater 565:153735

2. Wang YC, Dong X, Liu YH, Liu YH, Cao XH, Chen J, Xu C (2020) Electrochemical and spectrochemical analysis of U(VI) reduction in nitric acid solutions. Electroanal Chem 874:114482

3. Ding L, Wang XP, Yan YD, Smolenski V, Xu WD, Novoselova A, Xue Y, Ma FQ, Zhang XM (2022) Electroextraction of neodymium from LiCl-KCl melt by using binary liquid Ga-Al cathode. J Rare Earth. https://doi.org/10.1016/j.jre.2022.04.022

4. Liu YL, Yan YD, Han W, Zhang ML, Yuan LY, Liu K, Ye GA, He H, Chai ZF, Shi WQ (2013) Extraction of thorium from LiCl-KCl molten salts by forming Al-Th alloys: a new pyrochemical method for the reprocessing of thorium-based spent fuels. RSC Adv 3(45):23539–23547

5. Park W, Choi EY, Kim SW, Jeon SC, Cho YH, Hur JM (2016) Electrolytic reduction of a simulated oxide spent fuel and the fates of representative elements in a Li$_2$O-LiCl molten salt. J Nucl Mater 477:59–66

6. Breza J, Darílek P, Necas V (2010) Study of thorium advanced fuel cycle utilization in light water reactor VVER-440. Ann Nucl Energy 37(5):685–690

7. Liu YL, Lan JH, Wang L, Jiang SL, Liu YC, Zhong YK, Yang DW, Zhang L, Shi WQ (2022) The influence of F$^-$ ion on the electrochemical behavior and coordination properties of uranium in LiCl-KCl molten salt. Electrochim Acta 404:139573

8. Yang DW, Jiang SL, Liu YL, Geng JS, Li M, Wang L, Chai ZF, Shi WQ (2021) Electrochemical extraction kinetics of Nd on reactive electrodes. Sep Purif Technol 281:119853

9. Wang DD, Liu YL, Yang DW, Zhong YK, Han W, Wang L, Chai ZF, Shi WQ (2022) Separation of uranium from lanthanides (La, Sm) with sacrificial Li anode in LiCl-KCl eutectic salt. Sep Purif Technol 292:121025

10. Park JW, Cha HL, Yun JI (2022) Electrochemical behaviors and thermodynamic properties of Ce on liquid Bi, Sn, and Zn electrodes in molten LiCl-KCl salt. J Electrochem Soc 169(4):043517

11. Yan YD, Xu YL, Zhang ML, Xue Y, Han Y, Huang Y, Chen Q, Zhang ZJ (2013) Electrochemical extraction of neodymium by co-reduction with aluminum in LiCl-KCl molten salt. J Nucl Mater 433(1–3):152–159

12. Yin TQ, Xue Y, Yan YD, Ma ZC, Ma FQ, Zhang ML, Wang GL, Qiu M (2021) Recovery and separation of rare earth elements by molten salt electrolysis. Int J Miner Metall Mater 28:899–914

13. Willimson MA, Willit JL (2011) Pyroprocessing flowsheets for recycling used nuclear fuel. Nucl Eng Technol 43(4):329–334

14. Inoue T, Koyama T, Arai Y (2011) State of the art of pyroprocessing technology in Japan. Energy Procedia 7:405–413

15. Mcfarlane HF, Lineberry MJ (1997) The IFR fuel cycle demonstration. Prog Nucl Energy 31(1):155–173

16. Zhong YK, Liu YL, Liu K, Wang L, Li M, Gibson JK, Chen JZ, Jiang SL, Liu YC, Yuan LY (2021) In-situ anodic precipitation process for highly efficient separation of aluminum alloys. Nat Commun 12(1):5777

17. Kim JH, Lee BO, Lee CB, Jee SH, Yoon YS (2012) Formation of intermetallic compound at interface between rare earth elements and ferritic-martensitic steel by fuel cladding chemical interaction. J Rare Earths 30(6):599–603

18. Kuznetsov SA, Hayashi H, Minato K, Escard MG (2006) Electrochemical transient techniques for determination of uranium and rare-earth metal separation coefficients in molten salts. Electrochim Acta 51(12):2463–2470

19. Toda T, Maruyama T, Moritani K, Moriyama H, Hayashi H (2009) Thermodynamic properties of lanthanides and actinides for reductive extraction of minor actinides. J Nucl Sci Technol 46(1):18–25

20. Xi XL, Liu QQ, Nie ZR, Li M, Ma LW (2018) Electrochemical preparation of tungsten and cobalt from cemented carbide scrap in NaF-KF molten salts. Int J Refract Met H 70:77–83

21. Li WL, Han W, LiM, Zhang YC, Zhang YC, Yue MT, Sun Y (2021) Electroreduction of Dy(III) assisted by Zn and its co-deposition with Zn(II) in LiCl-KCl molten salt. Appl Organomet Chem 34(10):5817–1–5817–13

22. Wang YC, Li M, Han W, Zhang ML, Jiang T, Peng SM, Yan YD (2016) Electrochemical behaviour of erbium(III) and its extraction on Cu electrode in LiCl-KCl melts. J Alloy Compd 695:3484–3494

23. Wang CX, Chen JS, Li BC, Zhao H, Jin BJ, Liu KR, Han Q (2021) Cathodic behavior of scandium(III) on reactive copper electrode in LiF-CaF$_2$ eutectic molten salt. J Rare Earth 40(10):1641–1650

24. Wang YC, Mei Li, Zhang ML, Han W, Jiang T, Yan YD (2018) Electrochemical deposition of praseodymium (III) and copper (II) and extraction of praseodymium on copper electrode in LiCl-KCl melts. J Solid State Electr 22(12):3689–3702

25. Han W, Li ZY, Li M, Gao YY, Yang XG, Zhang ML, Sun Y (2018) Electrolytic extraction of dysprosium and thermodynamic evaluation of Cu-Dy intermetallic compound in eutectic LiCl-KCl. RSC Adv 8(15):8118–8129

26. Liu K, Liu YL, Yuan LY, Wang L, Li ZJ, Chai ZF, Shi WQ (2018) Thermodynamic and electrochemical properties of holmium and Ho$_x$Al$_y$ intermetallic compounds in the LiCl-KCl eutectic. Electrochim Acta 174:15–25

27. Li M, Gu QQ, Han W, Yan YD, Zhang ML, Sun Y, Shi WQ (2015) Electrodeposition of Tb on Mo and Al electrodes: thermodynamic properties of TbCl$_3$ and TbAl$_2$ in the LiCl-KCl eutectic melts. Electrochim Acta 167:139–146

28. Su LL, Liu K, Liu YL, Wang L, Yuan LY, Wang L, Li ZY, Zhao XL, Chai ZF, Shi WQ (2014) Electrochemical behaviors of Dy(III) and its co-reduction with Al(III) in molten LiCl-KCl salts. Electrochim Acta 147:87–95

29. Liu K, Liu YL, Yuan LY, Zhao XL, He H, Ye GA, Chai Z, Shi WQ (2014) Electrochemical formation of erbium-aluminum alloys from erbia in the chloride melts. Electrochim Acta 116:434–441

30. Ji DB, Yan YD, Zhang ML, Wang P, Yang X, Jiang XY, Xue Y, Han W, Hartmann T (2015) Study on electrochemical behavior of La(III) and preparation of Al-La intermetallic compound whiskers in chloride melt. J Electrochem Soc 163(2):D1–D8

31. Castrillejo Y, Fernández P, Medina J, Hernandez P, Barrado E (2011) Electrochemical extraction of samarium from molten chlorides in pyrochemical processes. Electrochim Acta 56(24):8638–8644

32. Tang H, Yan YD, Zhang ML, Li X, Han W, Xue Y, Zhang ZJ, He H (2013) Fabrication of Mg-Pr and Mg-Li-Pr alloys by electrochemical co-reduction from their molten chlorides. Electrochim Acta 107:209–215

33. Li X, Yan YD, Zhang ML, Tang H, Ji DB, Han W, Xue Y, Zhang JL (2014) Electrochemical reduction of Tm on Mg electrodes and co-reduction of Mg, Li and Tm on W electrodes. Electrochim Acta 135:327–335

34. Chen Y, Ye K, Zhang ML (2010) Preparation of Mg-Yb alloy film by electrolysis in the molten LiCl-KCl-YbCl$_3$ system at low temperature. J Rare Earth 28(1):128–133

35. Jiang T, Wang N, Peng SM, Li M, Han W, Zhang ML (2016) Electrochemical formation of Mg-Lu alloy and alloy layer in molten LiCl-KCl. J Alloy Compd 658:198–209

36. Iida T, Nohira T, Ito Y (2001) Electrochemical formation of Sm-Ni alloy films in a molten LiCl-KCl-SmCl$_3$ system. Electrochim Acta 46(16):2537–2544

37. Wang SS, Li M, Han W (2019) Selective formation of Ce-Ni hydrogen storage alloys by electrodeposition in LiCl-KCl-CeCl$_3$ melts using Ni as cathode. J Alloys Compd 777:1211–1221

38. Iida T, Nohira T, Ito Y (2003) Electrochemical formation of Yb-Ni alloy films by Li codeposition method in a molten LiCl-KCl-YbCl$_3$ system. Electrochim Acta 48(11):1531–1536

39. Zheng JN, Yin TQ, Wang P, Yan YD, Smolenski V, Novoselova A, Zhang ML, Ma FQ, Xue Y (2022) Electrochemical extraction of ytterbium from LiCl-KCl-YbCl$_3$-ZnCl$_2$ melt by forming Zn-Yb alloys. J Solid State Electr 26:1067–1074

40. Liu YL, Zhou W, Tang HB, Liu ZR, Liu K, Yuan LY, Feng YX, Chai ZF, Shi WQ (2016) Diffusion coefficient of Ho^{3+} at liquid zinc electrode and co-reduction behaviors of Ho^{3+} and Zn^{2+} on W electrode in the LiCl-KCl eutectic. Electrochim Acta 211:313–321

41. Han W, Li WL, Li M, Li ZY, Sun Y, Yang XG, Zhang ML (2018) Electrochemical co-reduction of Y(III) and Zn(II) and extraction of yttrium on Zn electrode in LiCl-KCl eutectic melts. J Solid State Electrochem 22(8):2435–2444

42. Liu K, Liu YL, Chai ZF, Shi WQ (2017) Evaluation of the electro-extractions of Ce and Nd from LiCl-KCl molten salt using liquid Ga electrode. J Electrochem Soc 164(4):D169–D178

43. Wang YC, Liu Q, Zhang S, Liu YH, Wang YQ, Dai Y, Dong ZM, Cheng ZP, Cao XH, Chen YQ (2022) Electrolytic extraction of yttrium using recycle liquid gallium electrode from molten LiCl-KCl. Sep Purif Technol 294:120972

44. Li B, Liu K, Pang JW, Yuan LY, Liu YL, Lin MZ (2018) Electrochemical properties of gadolinium on liquid gallium electrode in LiCl-KCl eutectic. J Rare Earths 36:656–661

45. Han W, Li ZY, Li M, Li WL, Zhang XM, Yang XG, Zhang ML, Sun Y (2017) Electrochemical extraction of holmium and thermodynamic properties of Ho-Bi alloys in LiCl-KCl eutectic. J Electrochem Soc 164(4):E62–E70

46. Li M, Liu YC, Sun ZX, Han W, Zhang ML, Yang XG, Sun Y (2019) Electrochemical co-reduction of Bi(III) and Y(III) and extracting yttrium from molten LiCl-KCl using liquid Bi as cathode. Chem Res Chinese U 35:60–64

47. Li M, Gu QQ, Han W, Zhang XM, Sun Y, Zhang ML, Yan YD (2015) Electrochemical behavior of La(III) on liquid Bi electrode in LiCl-KCl melts. Determination of thermodynamic properties of La-Bi and Li-Bi intermetallic compounds. RSC Adv 5(100):82471–82480

48. Li M, Sun ZX, Han W, Sun Y, Yang XG, Wang W (2020) Electrochemical reaction of Sm (III) on liquid Sn electrode. J Electrochem Soc 167(2):022502

49. Han W, Wang W, Zhang YQ, Wang WJ, Li M, Sun Y (2021) Electrode reaction of Pr on Sn electrode and its electrochemical recovery from LiCl-KCl molten salt. Int J Energ Res 45(6):8577–8592

50. Li ZY, Liu ZR, Li WL, Han W, Li M, Zhang ML (2020) Electrochemical recovery of dysprosium from LiCl-KCl melt aided by liquid Pb metal. Sep Purif Technol 250:117124

51. Li ZY, Tang DD, Meng SY, Gu LH, Dai Y, Liu ZR (2021) Electrolytic separation of Dy from Sm in molten LiCl-KCl using Pb-Bi eutectic alloy cathode. Sep Purif Technol 276:119045

52. Han W, Li WL, Chen JZ, Li M, Li ZY, Dong YC, Zhang ML (2019) Electrochemical properties of yttrium on W and Pb electrodes in LiCl-KCl eutectic melts. RSC Adv 9(46):26718–26728

53. Li M, Sun ZX, Guo D, Han W, Sun Y, Yang XG, Zhang ML (2020) Electrode reaction of Pr(III) and coreduction of Pr(III) and Pb(II) on W electrode in eutectic LiCl-KCl. Ionics 26(8):3901–3909

54. Castrillejo Y, Hernandez P, Fernandez R, Barrado E (2014) Electrochemical behaviour of terbium in the eutectic LiCl-KCl in Cd liquid electrodes. Evaluation of the thermochemical properties of the TbCd$_x$ intermetallic compounds. Electrochim Acta 147:74–751

55. Yin TQ, Liu YL, Wang L, Yan YD, Wang GL, Chai ZF, Shi WQ (2019) Thermodynamic properties of praseodymium on the liquid cadmium electrode and evaluation of anodic dissolution behavior in LiCl-KCl eutectic. J Nucl Mater 523:16–25

56. Yoon D, Phongikaroon S, Zhang JS (2016) Electrochemical and thermodynamic properties of CeCl$_3$ on liquid cadmium cathode (LCC) in LiCl-KCl eutectic salt. J Electrochem Soc 163(3):E97–E103

57. Jiao SQ, Jiao HD, Song WL, Wang MY, Tu JG (2020) A review on liquid metals as cathodes for molten salt/oxide electrolysis. Int J Min Met Mater 27(12):1588–1598

58. Han W, Li WL, Li M, Yang ZQ, Chen LY, Zhang YC, Meng YY, Li QB, Sun Y (2020) Electrochemical extraction of metallic Y using solid and liquid double cathodes. Electrochim Acta 346:136233

59. Yang YS, Zhang ML, Han W, Sun PY, Liu B, Jiang HL, Jiang T, Peng SM, LiM YK, Yan YD (2014) Selective electrodeposition of dysprosium in LiCl-KCl-GdCl$_3$-DyCl$_3$ melts at magnesium electrodes: application to separation of nuclear wastes. Electrochim Acta 118:150–156

60. Bard AJ, Faulkner LR (2001) Electrochemical methods: fundamentals and applications. Wiley, New York

61. Castrillejo Y, Bermejo MR, Barrado AI (2005) Electrochemical behaviour of dysprosium in the eutectic LiCl-KCl at W and Al electrodes. Electrochim Acta 50(10):2047–2057

62. Wang YF, Zhou WT, Guo SQ, Zhang JS (2017) Thermodynamic properties of fission products (Pr, Ce, Er) in liquid bismuth by thermodynamic assessment. J Nucl Mater 495:181–191

63. Yin TQ, Liang Y, Qu JM, Li P, An RF, Xue Y, Zhang ML, Han W, Wang GL, Yan YD (2017) Thermodynamic and electrochemical properties of praseodymium and the formation of Ni-Pr intermetallics in LiCl-KCl melts. J Electrochem Soc 164(13):D835–D842

64. Marsden KC, Pesic B (2011) Evaluation of the electrochemical behavior of CeCl$_3$ in molten LiCl-KCl eutectic utilizing metallic Ce as an anode. J Electrochem Soc 158(6):F111–F120

65. Tang H, Pesic B (2014) Electrochemistry of ErCl$_3$ and morphology of erbium electrodeposits produced on Mo substrate in early stages of electrocrystallization from LiCl-KCl molten salts. Electrochim Acta 133:224–232

66. Konishi H, Nohira T, Ito Y (2002) Morphology control of Dy-Ni alloy films by electrochemical displantation. Electrochem Solid St 5(12):B37–B39